University of Petroleum /CNPC Key Lab

12iwsa-wei.doc

Mar 2007

Effect of fracture scale length and aperture on seismic wave propagation: An experimental study

Jianxin Wei[1], *Bangrang Di*[1] *and Xiang-Yang Li*[2]

[1] CNPC Key lab of Geophysical exploration , China University of Petroleum , Beijing , China
[2] British Geological Survey, West Mains Road, Edinburgh EH9 3LA, UK
*

Paper presented at the 12th International Workshop on Seismic Anisotropy – Beijing, 22-25th October 2006

Suggested short title: ***Effects of fracture parameters on seismic waves***

Intended publication: *Journal of Applied Geophysics*

Submitted on *27 March 2007*

Revised on

***Address for correspondence**
Xiang-Yang Li
Britigh Geological Survey
Murchison House,
West Mains Road
Edinburgh EH9 3LA
Scotland,UK

xyl@bgs.ac.uk

Abstract

In this paper, we investigate the effects of fracture scale length and aperture on seismic wave propagation through seismic physical modelling. The physical models are constructed from a solid background of epoxy resin with inclusions of silicon rubber chips which come with different radius and thickness to simulate fractures with different scale length and aperture. The chips embedded in each model are of the same radius and thickness, and the fracture density is kept constant for all models in order to understand the effects of the scale length and aperture. P and S waves that propagate parallel and perpendicular to the fractures are then recorded using a pulse transmission method. The experimental results show that given the same fracture density the changing of radius has an only minor effect on the P-wave velocity and amplitude, and there are also little effects on the shear-wave amplitudes. The main observable effect is an increase of the slow shear-wave velocity with radius, leading to a decrease in shear-wave splitting with radius. The changing of fracture thickness has also little effects on the shear-wave amplitude except an obvious decrease in the slow shear-wave velocity, leading to an increase of shear-wave splitting with thickness. However, the increasing in fracture thickness induced a strong attenuation in the P-wave, in particularly for P-wave propagating perpendicular to the fracture. These findings may be useful for differentiating the effects of thin microcracks and large open fractures.

Keywords: Seismic physical modelling, fracture aperture, fracture scale length

---

1. Introduction

Equivalent medium theories, such as Hudson (1980) and Liu et al. (2000), are often used to model seismic wave propagation in fractured media. These theories can effectively describe the effects of fracture density and orientation, as well as multiple fracture sets, but they cannot account for the effects of fracture scale length and aperture, which become increasingly important for fractured reservoir characterization. Chapman (2003) extended the existing equivalent medium theories to account for the effects of fracture scale length, and some of the predicted frequency-dependent effects have subsequently confirmed by field data (e.g. Maultzsch et al. 2003). However, there is still a lack of understanding on the effects of fracture aperture. Here, through experiment studies in the laboratory with controlled fracture models and seismic physical modelling, we aim to investigate the effect of different fracture scale length and aperture on seismic velocity and amplitude.

Several approaches have been reported in the literature to study the effects of fracture parameters on seismic waves through seismic physical modelling in laboratories. One is to construct the fractured models through superposition of thin chips of fractured material, and the fracture density is represented by the number of chips in one wavelength (e.g, Tatham et al., 1992; Ebrom et al., 1990; He et al., 2001). The other method is to embed round chips of a known number into a background material and the corresponding relationship between the fracture density and seismic wave velocities and anisotropy parameters can then be calculated using the equivalent medium theory (e.g., Ass'ad et al., 1992; Rathore et al., 1995; Wei, 2004). Another method is to simulate anisotropic media by using industrial materials such as phenolic resin or epoxy resin (Cheadle et al., 1991; Isaac et al., 1999; Wang et al., 2007). However, these studies were designed only to study the effects of fracture density; the effects of fracture scale length and aperture have not been addressed.

In this paper, the embedding method with round chips, as in Wei (2004), is adopted. Fracture models with different fracture radius, or diameter (scale length) and thicknesses (aperture) but with the same fracture density are constructed and the pulse transmission method is used to study the effects on seismic wave (e.g. travel time, amplitude and frequency).

2. Experimental procedures

This is to explain how the fracture models are constructed and how the P- and S-waves are measured.

2.1 Fracture Model Construction

The construction is based on Hudson's (1980) theoretic hypothesis of thin penny-shaped fractures. The models consist of a solid base with inclusions of low velocity thin penny-shaped materials (Fig. 1). For each model, the fracture density (ε) is given by $\varepsilon = Nr^3/V$, where V denotes the volume of the base material, r denotes the radius of the round chips and N is the total number of chips in the base material. The fracture density changes when we alter N or r. We can keep the fracture densities constant if we change N or r proportionally in the same time. Two sets of fractured models are constructed: one set with varying fracture radius, and the other set with varying thickness, and the fracture density remains constant for each set (Tables 1 and 2).

All the models are constructed from a solid base of epoxy resin. The density of the base material is 1.18g/cm^3; the P-wave velocity is 2630m/s and the S-wave velocity is 1200m/s. The round chip simulating a fracture is made from a mixture of silicon rubber. A large block of this mixture is made first and the block size is (400x200x30mm); round chips of different radius and thickness are then cut from the block. The density and velocity of the chip inclusions are measured from the block mixture: the density is 1.09 g/cm^3, and the P-wave velocity is 1360m/s. There is no S-wave signal received from this rubber mixture, and this is likely due to the fact that the block mixture is too soft to propagate shear-waves. Therefore, we may consider its shear-wave velocity as zero. From the cutting process, we found that it is relatively easier to control chip radius than thickness. Chips of the same thickness have to be carefully selected from a large numbers of chips which have similar thickness.

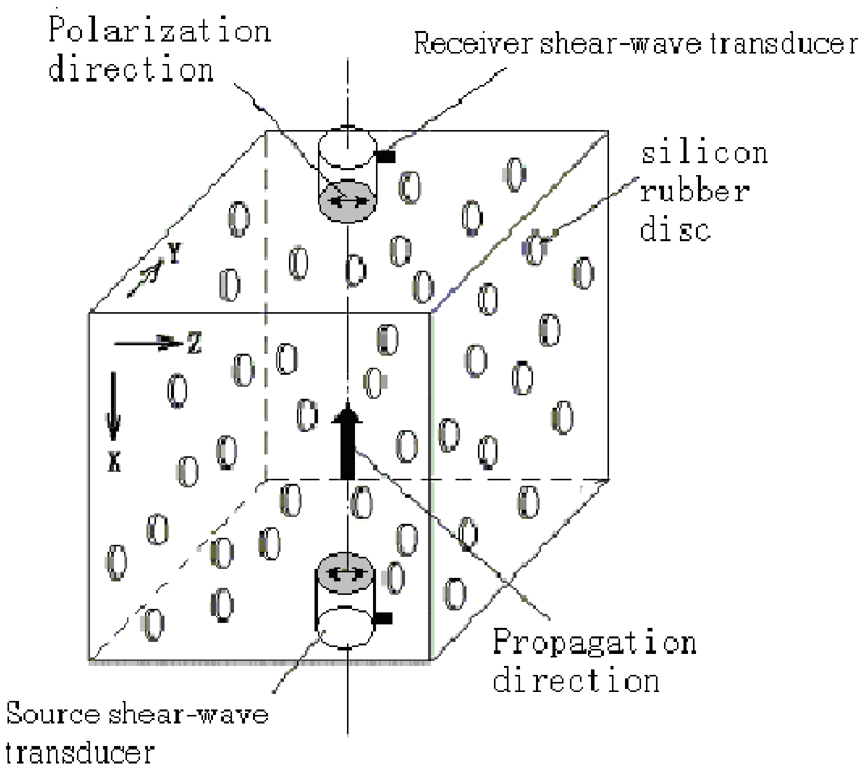

Fig. 1. Schematic diagrams of the controlled fracture model using epoxy resin and round chips of silicon rubber.

Each fractured model is made of 35 layers of epoxy resin with equal weight to ensure that the separation between two neighbouring layers is kept the same. The thickness of each layer is 1.72mm. Once a layer is laid, silicon rubber chips with random distribution are embedded into the layer, and another layer of epoxy resin is then added on the top. This process is repeated, and the total embedded chip layers are 34. The whole process is very tedious and labour intensive. These chip layers simulate fractures with preferred directions along the X- and Y-axis and with fracture normal along the Z-axis direction. Note that to simulate vertical fracture, the block is rotate so that the Z-axis is no longer at the vertical direction (Fig. 1).

Table 1. List of geometrical parameters of the fracture models with different diameter (radius). The average thickness for Models 1-6 is 0.14mm.

Model No.	Crack diameter (mm)	Model sides（cm） X×Y×Z	Volume(cm^3)	Number of cracks / layer	Total number of cracks	Cracks density（%）
0	N/A	70.14×70.14×57.3	276	0	0	0
1	**2.5**	**70.35×69.92×57.32**	**282**	**313**	**10642**	**7.37**
2	**3.0**	**70.34×69.92×57.3**	**282**	**181**	**6154**	**7.37**
3	**3.5**	**70.4×69.86×57.32**	**282**	**114**	**3876**	**7.37**
4	**4.2**	**70.34×69.9×57.28**	**282**	**66**	**2244**	**7.38**
5	**5.0**	**70.38×69.92×57.3**	**282**	**39**	**1326**	**7.35**
6	**6.0**	**70.32×69.88×57.3**	**282**	**23**	**782**	**7.5**

Table 2. List of geometrical parameters of the fracture models with different thickness. The average radius for the six models is 2.1mm.

Model No.	Cracks thickness (mm)	Model sides（cm） X×Y×Z	Volume(cm^3)	Number of cracks / layer	Total number of cracks	Cracks density（%）
1	**0.1**	**70.58×70.2×58.02**	**287**	**70**	**2380**	**7.67**
2	**0.14**	**70.54×70.22×58.0**	**287**	**70**	**2380**	**7.67**
3	**0.2**	**70.52×70.16×58.0**	**287**	**70**	**2380**	**7.68**
4	**0.24**	**70.48×70.25×58.0**	**287**	**70**	**2380**	**7.68**
5	**0.29**	**70.58×70.12×57.98**	**287**	**70**	**2380**	**7.68**
6	**0.34**	**70.54×70.14×57.98**	**287**	**70**	**2380**	**7.68**

Each model is shaped into a cube with parallel and smooth surfaces to ensure good coupling condition between transducers and model surface and also to ensure that the volume of the model can be calculated accurately. Due to the construction process, the model dimmensions can vary slightly from 6.5cm to 7cm. The density obtained from the model without fractures is 1.18g/cm^3. Tables 1 and 2 list the fracture parameters for the two sets of models. There are seven models in Table 1, of which model 0 is the model without fractures and the others six models have different fracture radius. The fracture density is about 0.074 and the average fracture thickness is 0.14mm for the six fractured models in Table 1. Table 2 lists the six models with constant fracture radius but varying fracture thickness. The average fracture radius is 2.1mm for the six models in Table 2, and their mean thickness distribution is shown in Fig. 2. Due to the heterogeneities in the mixture of silicon rubber, it is difficult to control the thickness. Therefore, a tolerance of 0.05mm is set for the thickness to vary in each fracture model in Table 2.

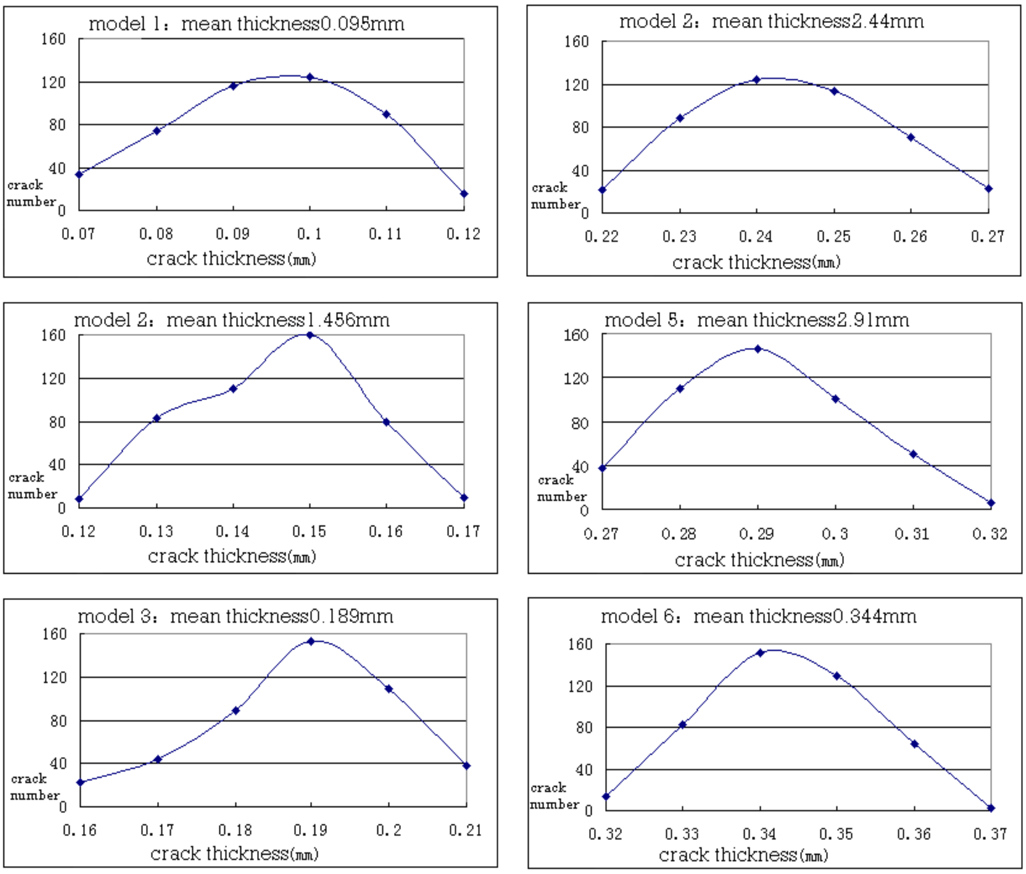

Fig. 2. The mean distribution of fracture thickness for the six models listed in Table 2.

2.2 P-wave and S-wave recording

The pulse transmission method is used to measure P and S wave velocities for all the models for the direction parallel (X-axis) and perpendicular (Z-axis) to the fracture chips. The receiver transducer is placed against the top surface of the model, and the source transducer was placed directly below the receiver against the bottom surface of the model, as shown in Fig. 1. Measurements of the first arrival time together with a determination of the path length are sufficient to calculate the wave velocity. And the waveforms can also be recorded. The transducer in the experiment has the characteristics of broad bandwidth and short pulse. The S-wave transducer has good polarization direction. The centre frequency of P-wave transducer is 200kHz and the bandwidth is 100kHz to 300kHz. The centre frequency of S-wave transducer is 100kHz and the bandwidth is 60kHz to 250kHz. The wavelength of the P- and S-waves generated in the experiment is 20 to 30mm, which is much larger than the fracture radius, and approximately satisfies the long wavelength assumptions of the equivalent medium theories.

This initial experiment is designed mainly to compare the anisotropic properties of the fracture models of identical fracture density but different fracture radius or thicknesses. The P- and S-wave measurements are only done in the direction of parallel and perpendicular to the fracture. The common-polarization transmission technique is adopted in the S-wave measurement. Two transducers have the same polarization direction. When the S-wave propagates along the X direction, and the polarization is parallel to the fracture, this S-wave is referred as the fast shear-wave (S1), and when the polarization is perpendicular to the fracture, the wave is referred to as the slow shear-wave (S2). When the S-wave propagates along the Z-direction, the shear-wave polarized at the X-direction is referred to as Sx, and the one plarized at the Y-direction is referred to as Sy. The errors in the measurements are kept within 2%.

3. Experimental results

Before experimenting on the models with fractures, we first examine the elastic properties of the background material of model 0 in Table 1. Fig. 3 shows the recorded P-wave and S-waves with two polarization directions (parallel and perpendicular to the epoxy layering) at the propagation direction of X-axis. P-wave velocity is 2624m/s and the two S-wave velocities are 1198m/s and 1198m/s. The two S-wave velocities are identical, indicating no shear-wave splitting in the background material, and waveforms of the two shear-waves are also very similar except for some minor differences in the tail of the wavelet. This confirms that the construction process of the background material does not induce artificial anisotropic effects into the models. This also agrees with the characteristics of the frequency spectra, as shown in Fig. 3, from which we can also estimate the dominate wavelength of the P- and S-waves, as 13.6mm and 11.8mm, respectively. Therefore, the long wavelength assumption is not strictly satisfied when the fracture radius is greater than 4mm.

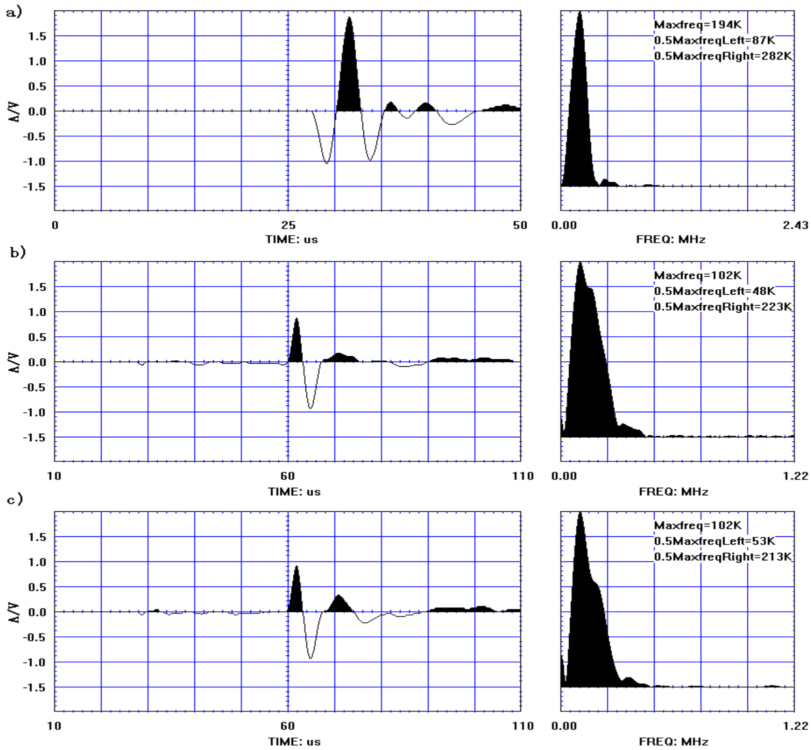

Fig. 3. Waveforms recorded for the model without fractures (model 0 in Table 1): a) the P-wave and its corresponding frequency spectra; b) S-wave polarized at the direction of Y-axis, parallel to the layering and its corresponding frequency spectra; and c) S-wave polarized at the direction of Z-axis, perpendicular to the layering and its corresponding frequency spectra.

Figs. 4-9 show the P- and S-wave recorded for all the fractured models in Tables 1 and 2, and their corresponding velocities are summarized in Tables 3 and 4. We will discuss the P- and S-wave results separately in the following sections.

3.1 P-wave results

Figs. 4 and 5 shows the P-wave records for the two sets of fracture models in Tables 1 and 2 at the propagation direction of X-axis (parallel to the fractures) and Z-axis (perpendicular to the fractures), and the corresponding P-wave velocities are listed in Tables 3 and 4.

In Fig. 4a, the fracture diameter (scale length) increases from 2.5mm to 6mm, and the P-wave travel time decreases from 27.3μs to 26.9μs .The variation in 0.4μs(about 1.5%), and this larger than the measurement error which is ±0.1μs. This indicates that the P-wave velocity parallel to the fracture strike increases with increasing crack radius. Furthermore, there is little variation in the waveforms in Fig. 4a, suggesting that the change of radius within the long wavelength assumption for non-saturated cracks has negligible effects on the P-wave amplitude. There is a 14% reduction in magnitude in Fig. 4a for a 2.4 times increasing in fracture radius. For P-wave travelling perpendicularly to the fractures (Z-axis), there is a 1.5% reduction in P-wave velocity (Table 3), and a slight decrease in the P-wave amplitude (Fig. 4b), compared with the P-waves parallel to the fractures in Fig. 4a. At the propagating direction along Z-axis, the effects of varying fracture radius has little effects on the P-wave velocity, and its effects on amplitude is also small (Fig. 4b).

In contrast, changes of thickness have a stronger effect on the P-wave, as shown in Fig. 5. At the direction parallel to the fracture, there is a small variation of 1.1% in the P-wave velocity for a 3.4 times changes in fracture aperture. However, there are very significant changes in the P-wave amplitude and waveforms. As the fracture aperture increases, the P-wave is substantially attenuated, as shown in Fig. 5a. For a 3.4 times change in fracture aperture, there is 3.8 times reduction in P-wave amplitude, and the higher frequencies are also attenuated with a shift to low frequency (Fig. 5a). These effects are even more significant for the P-waves propagating at the perpendicular direction, as shown in Fig. 5b. The P-wave velocities have changes up to 3% (Table 4), and the effects on the amplitude are also more than doubled (Fig. 5b). This shows a clear link between P-wave attenuation and variations of fracture aperture.

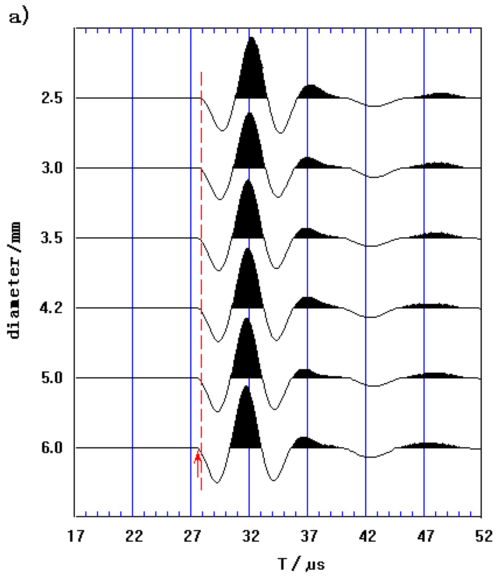

(a) Parallel

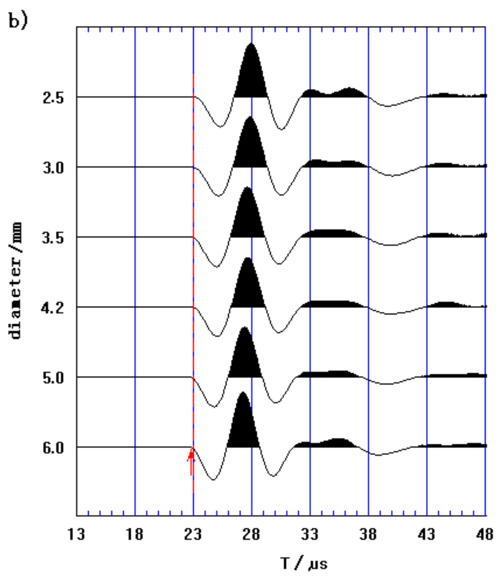

(b) Perpendicular

Fig. 4. Comparison of P-waves recorded for the fractured models with different diameter in Table 1, propagating (a) parallel and (b) perpendicular to the fractures.

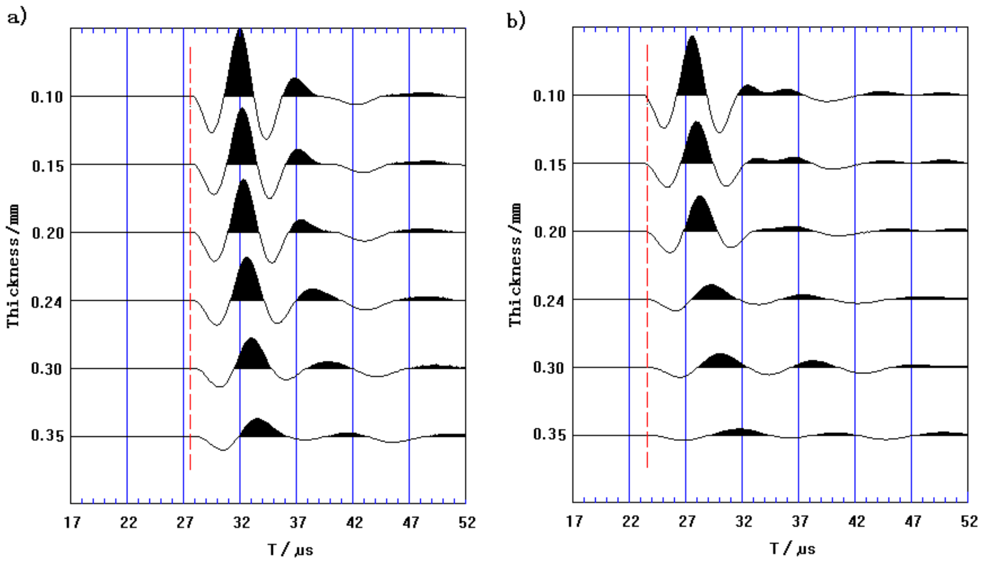

(a) Paralle (b) Perpendicular

Fig. 5. Comparison of P-waves recorded for the fractured models with different thickness in Table 2, propagating (a) parallel and (b) perpendicular to the fractures.

Table 3. Measured seismic velocities and Thomsen (1986) parameter γ for the models in Table 1 with different fracture diameter. The fracture thickness is kept at 0.14mm.

Model No.	Fracture diameter (mm)	Vp-X (m/s)	Vp-Z (m/s)	Vs – X (m/s)		Vs -Z (m/s)		γ -X (%)	γ -Z (%)
				S1	S2	Sx	Sy		
1	2.5	2577	2559	1181	1094	1137	1133	7.37	0.3
2	3.0	2586	2560	1183	1108	1141	1137	6.34	0.4
3	3.5	2588	2562	1187	1115	1142	1142	6.07	0
4	4.2	2596	2572	1187	1106	1141	1141	6.83	0
5	5.0	2607	2575	1189	1123	1146	1151	5.55	0.4
6	6.0	2614	2580	1190	1123	1151	1146	5.63	0.4

3.2 S-wave results

For propagating at the X-direction, we have recorded the both the fast shear-wave (S1) and the slow shear-wave (S2). For propagating at the Z-direction, we have also recorded both Sx and Sy. This is to check the symmetry of the material. For a material with transverse isotropy, Sx and Sy will have the same velocity as S2, but their polarizations are parallel to the fracture as in S1.

Fig. 6 shows the fast S1 and slow S2 waves for the fractures models in Table 1 with varying fracture radius. Similar to the P-waves, the changes in fracture radius has almost no effects on the velocity of the fast waves (Fig. 6a and Table 3); the effect on the amplitude is also small; there is about 16% reduction in amplitude and the waveforms remain similar. The influence of fracture radius to slow S-wave velocity is evident and the velocity increases by 2.6% as the fracture radius increases (Table 3), whilst the amplitude decreased by 20%. There are some visible distortions to the S2 waveforms. When the radius is 3mm, noise signal can be observed before the onset of the slow waves due to scattering effects (Fig. 6b).

Fig. 7 shows the fast S1 and slow S2 waves for the fractures models in Table 2 with varying thickness. Contrary to the P-waves, changes in fracture thickness have a smaller influence on the shear-waves. S1 velocity shows almost no changes, and there is a 34% decrease in S1 amplitude (Table 4, Fig. 7a). The S1 waveforms also show little changes except for very large thickness. Some distortion and attenuation of higher frequency about 30% can be observed when the thickness is 0.35mm. The only obvious change is in the S2 velocity which decreases by 2.6%; surprisingly the S2 amplitudes also show little changes (Fig. 7b).

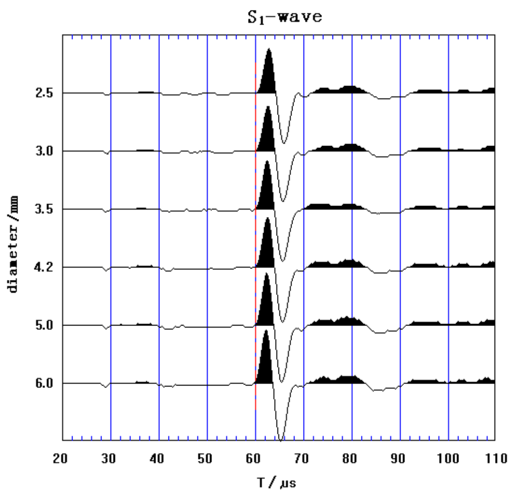

(a) Fast S1

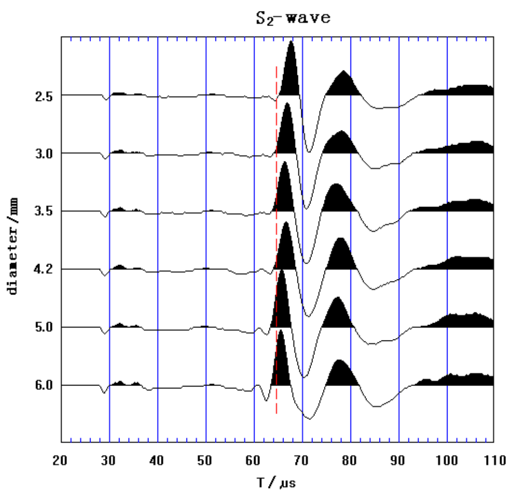

(b) Slow S2

Fig. 6. Comparison of (a) the fast S1 and the slow S2 waves recorded for the fractured models with different radius in Table 1, propagating parallel to the fractures along X-axis.

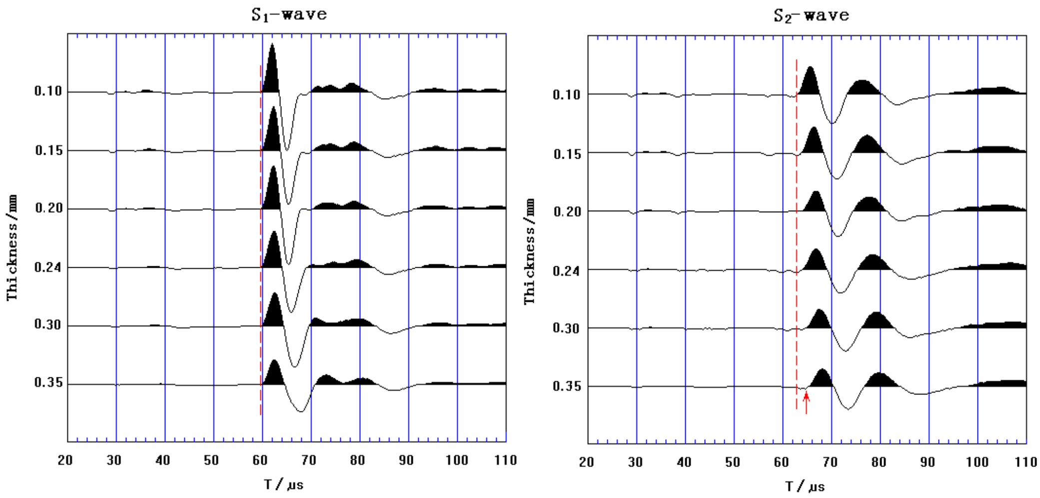

(a) Fast S1 (b) Slow S2

Fig. 7. Comparison of (a) the fast S1 and the slow S2 waves recorded for the fractured models with different thickness in Table 2, propagating parallel to the fractures along X-axis.

Table 4. Measured seismic velocities and Thomsen (1986) parameter γ for the models in Table 2 with different fracture thickness. The fracture radius is kept at 2.1mm.

Model No.	Thick-ness (mm)	Vp-X (m/s)	Vp-Z (m/s)	Vs-X (m/s)		Vs-Z (m/s)		γ-X (%)	γ-Z (%)
				S1	S2	Sx	Sy		
1	0.1	2620	2589	1198	1136	1156	1156	5.04	0
2	0.15	2610	2576	1198	1129	1151	1146	5.62	0.43
3	0.2	2605	2565	1197	1124	1146	1142	5.9	0.35
4	0.25	2601	2548	1199	1119	1137	1142	6.46	0.44
5	0.3	2594	2534	1201	1106	1141	1137	7.58	0.43
6	0.35	2590	2525	1201	1106	1141	1137	7.58	0.43

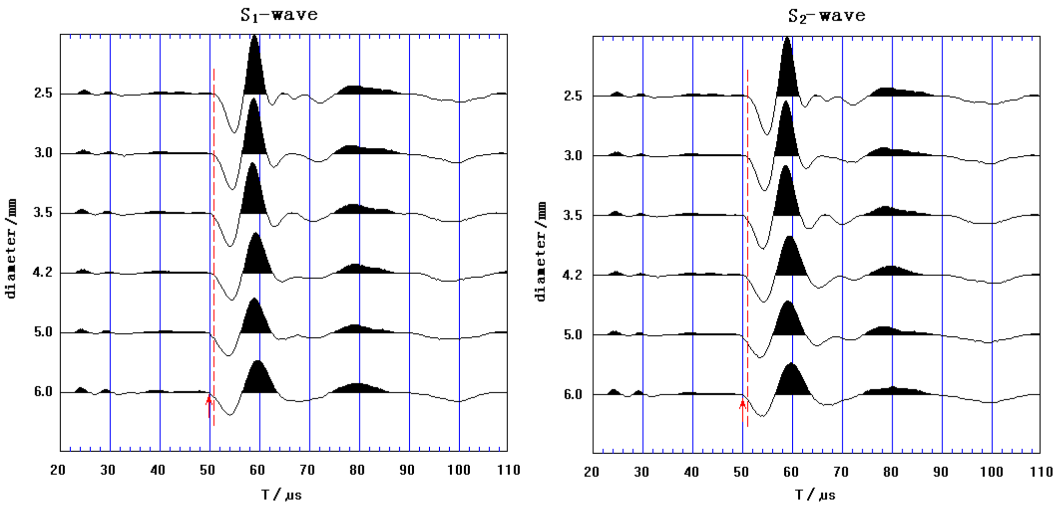

(a) Sx (b) Sy

Fig. 8. Comparison of the shear-waves polarized at (a) the X-direction (Sx) and (b) the Y-direction (Sy) for the fractured models with different radius in Table 1, propagating perpendicular to the fractures along Z-axis.

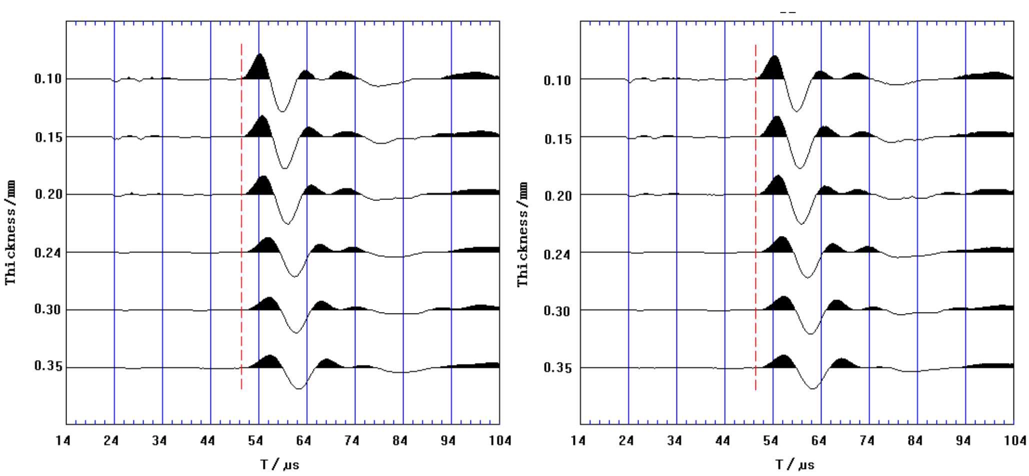

(a) Sx (b) Sy

Fig. 9. Comparison of the shear-waves polarized at (a) the X-direction (Sx) and (b) the Y-direction (Sy) for the fractured models with different thickness in Table 2, propagating perpendicular to the fractures along Z-axis.

The two shear-waves (Sx and Sy) recorded propagating perpendicularly to the fractures are very stable (Figs. 8 and 9). Their velocities are very much the same and the difference between them is very small. The effects of changes in fracture radius or thickness on these two waves are very similar to those on the S2, The trend of the variations is the same but with a smaller magnitude. For example, the S2 velocity increases with fracture radius in Fig. 6, and a similar increase can be observed in Fig. 8 but with a smaller magnitude. Also the S2 velocity decreases with fracture thickness in Fig. 7, and a similar decrease can also be observed in Fig. 9. This confirms that the fracture models possess transverse isotropy.

4. Discussion

As shown in Tables 3 and 4, the effects of changing fracture radius on P- and S-wave amplitude and waveforms are small. Some scattering effects can be observed only when the fracture diameter reaches 6mm. This may be due to fact the fracture scale length is much smaller compared with the wavelength and is still within the limits of the long wavelength assumption. The main effects of changing fracture radius are on the P and S-wave velocities. As the fracture radius increases, the P-wave velocity parallel to the fractures increases, but the P-wave velocity perpendicular to the fractures remains almost constant (Table 3). Therefore, there is an increase in the P-wave velocity anisotropy. There are possible two reasons for this. One is due to the changes of aspect ratio. As the fracture radius increases, the aspect ratio increases since the thickness remains constant at 0.14mm. This will increase the P-wave anisotropy as predicted by the equivalent medium theory such as Hudson (1980). The other reason may be due to scattering. As the fracture radius increases, the number of fractures decreases substantially in order to keep the fracture density constant. Therefore the total fracture area decreases. For example, the fracture area for the fracture model with a diameter of 2.5mm is 2.36 times larger than the fracture area in the fracture model with a diameter of 6mm due to a substantial reduction in the number of fractures. As a result, the fracture spacing will also increase. This will certainly reduce the scattering effects and increases the velocity.

Thomsen (1986) parameter (γ) is often used to examine the shear-wave anisotropy, which is often directly link to the fracture density (Li, 1997; 1998). The anisotropy parameter γ in Tables 3 and 4 can be calculated using the following formula,

$$\gamma = \frac{1}{2}\left(\frac{vs_1^2}{vs_2^2} - 1\right).$$

Therefore, the amount of shear-wave splitting as defined by γ decreases as the fracture diameter increases. Again this can be explained by the reduction in the number of fractures as fracture radius increases since the fracture density is kept constant, as in the P-wave case.

The P-waves suffer serious attenuation as the fracture aperture increases, and the P-wave attenuates more when propagates along the fracture normal then along the fracture strike. This is consistent with expectation. However, the S-wave shows little attenuation with increasing fracture thickness. This is likely induced by the material properties of the round chips which is not real fracture but a solid inclusion. This indicates that the using round chips of silicon rubber to simulate a fracture is probably more appropriate for P-wave propagation than for S-wave. Despite this, there is significant decreasing in S2 velocity, here an increasing in shear-wave splitting, as the fracture aperture increases. These observations may be useful in real data application.

Either changes in fracture radius or thickness have little effects on the shear-waves propagating along the fracture normal. This is probably due to the fact that both polarization of Sx and Sy are parallel to the fracture, and therefore they are relatively stable. This implies that for shear-waves, the wave polarized perpendicularly to the fractures is more sensitive to the changes in fracture parameters than the one parallel to the fractures regardless the propagating direction.

5. Conclusions

It is common to simulate fractured medium through embedding round chips with a low density and velocity into a solid background. Using this technique, we have constructed two sets of fracture models with fixed fracture density but with different fracture radius and aperture to study their effects on seismic wave propagation. The main findings of these experiments can be summarized as follows:

1) As the fracture radius varies from 1.25mm to 3mm, for a given fracture density and fracture thickness, the P-wave anisotropy increases from 1% to 2%, whilst the amount of shear-wave splitting decreases from 7.4% to 5.6%. In contrast, the changes in fracture radius have little effects on the P- and S-wave amplitude and waveforms.
2) As the fracture thickness (aperture) varies from 0.1mm to 0.35mm, for a given fracture density and given fracture radius the P-wave anisotropy increases from 1.2% to 2.5%, and amount shear-wave splitting increases from 5.0% to 7.6%.
3) The changes in the fracture aperture show a significant effect on the P-wave amplitude and waveform. The P-wave decreases by 3.8 times when the fracture aperture increases by 3.4 times. However, the effect on the S-wave amplitude is small.
4) The P-wave propagating and the shear-wave polarizing perpendicular to the fractures are more sensitive to the changing in fracture properties compared with the P- and S-

waves along parallel directions. This is in consistent with known theory and observation.

Acknowledgements

This work is supported by the CNPC international collaboration programme through the CNPC Geophysical Key Laboratory at the China University of Petroleum and the Edinburgh Anisotropy Project (EAP) of the British Geological Survey (BGS), and is published with the approval of all project partners and the Executive Director of BGS (NERC).

References

Ass'ad, J.M., Tatham, R.H. and McDonald, J.A., 1992. A physical model study of microfracture-induced anisotropy. Geophysics, **57**, 1562-1570.

Chapman, M. 2003. Frequency dependent anisotropy due to meso-scale fractures in the presence of equant porosity, Geophysical Prospecting, **51**, 369-379

Cheadle, S. P., Brown, R. J. and Lawton, D. C., 1991. Orthorhombic anisotropy: A physical seismic modeling study. Geophysics, **56**, 1603-1613.

Ebrom, D. A., Tatham, R.H., Sekharan, K. K., McDonald, J. A., and Gardner, G. H. F.， 1990. Hyperbolic traveltime analysis of first arrivals in an azimuthally anisotropic medium： A physical model study：Geophysics, **55**, 185-191.

He, Z., Li, Y., Zhang, F. and Huang, D., 2001. Different effects of vertically oriented fracture system on seismic velocities and wave amplitude. Computing techniques for geophysical and geochemical exploration，**23**(1), 1-5.

Hudson, J.A., 1980. Overall properties of a fractureed solid. Math Proc. Camb. Phil. Soc, **88**, 371-384.

Isaac, J. H. and Lawton, D. C., 1999. Image mispositioning due to dipping TI media: A physical seismic modeling study. Geophysics, **64**, 1230–1238.

Li, X.-Y., 1997. Fractural reservior delineating using multicomponent seismic data. Geophysical Prospecting, **54**, 39-64

Li, X.-Y., 1998. Processing PP and PS waves in multicomponent sea-floor data for azimuthal anisotropy: theory and overview, Procedding of the Eighth International Workshop on seismic Anisotropy (Revue De L'institut francia du petrole), **53**, 607-620

Liu, E., Hudson, J. A. and Pointer, T., 2000, Equivalent medium representation of fractured rock, J. Geophys. Res., **105**, No.B2, 2981-3000

Maultzsch, S., Chapman, M., Liu, E. and Li, X.-Y., 2003. Modelling frequency dependent seismic anisotropy in fluid-saturated rock with aligned fractures: implication of fracture size estimation from anisotropic measurements. Geophysical Prospecting, 2003, **51**, 381-392.

Rathore, J.S, Fjaer, E., Holt, R.M, and Renlie, L., 1995. P- and S-wave anisotropy of a synthetic sandstone with controlied fracture geometry. Geophys. Prosp., **43**, 711-728.

Tatham, R.H., Matthews, M.D., Sekharan, K.K., Wade, C.J. and Liro, L.M., 1992. A physical model study of shear-wave splitting and fracture intensity: Geophysics, **57**, 647-652.

Thomsen, L., 1986.

Wang, S., Li, X.-Y., Qian, Z., Di, B. and Wei, J. 2007. Physical modelling studies of 3D P-wave seismic for fracture detection. Geophy. J. Int. **168**, 745-756.

Wei, J., 2004. A physical model study of different fracture densityes: Journal of Geophysics and Engineering, **1**, 70-76.